20 **Appendix 4: Description of chlorite and illite thermobarometers**

21

22 We give below a short review of existing thermometers, before applying them.

23

24 **Chlorite thermometry**

25

26 **Empirical chlorite thermometers**

27 The pioneer chlorite thermometer proposed by Cathelineau and Nieva (1985) and refined by

28 Cathelineau (1988) is based on a linear increase of ^{IV}Al content with temperature, as observed

29 from the Salton Sea hydrothermal field, where the pressure gradient is negligible compared to

30 the thermal gradient. Cathelineau (1988) refined the first equation of Cathelineau and Nieva

31 (1985) as follows:

32

33 $T \, °C = 321.98 \, ^{IV}Al – 61.92$ (on a 14-oxygens anhydrous basis).

34

35 Several authors (e.g. Shau et al. 1990; De Caritat et al. 1993; Jiang et al. 1994; Essene and

36 Peacor 1995) have criticized the use of this equation as a thermometer, firstly because the

37 chlorite analyses used for the equation calibration were suspected to be contaminated by other

38 mineral phases, and secondly because the ^{IV}Al content of chlorite also depends on the bulk-

39 rock composition. The latter point implies that the thermometer should not been used for

40 other rock composition than that used for its calibration. In order to take bulk-rock

41 composition effects into account, Kranidiotis and McLean (1987) introduced a tentative

42 correction based on the $XFe = Fe/(Fe+Mg)$ ratio:

43

44 $T \, °C = 106 \, (^{IV}Al + 0.7 \, XFe) + 18$ (on a 28-oxygens anhydrous basis).

45

46   Jowett (1991) proposed a further modification of the above equation:

47

48   T °C = 319 (^{IV}Al + 0.1 XFe) – 69 (on a 14-oxygens anhydrous basis and XFe < 0.6).

49

50   Later studies by Hillier and Velde (1991; Eq.1), Zang and Fyfe (1995; Eq.2), and Xie et al.

51   (1997; Eq.3) confirmed the positive correlation between temperature and ^{IV}Al content, and led

52   to the proposition of new empirical relations constrained using various sets of natural data:

53

54   T °C ≈ 249.56 ^{IV}Al – 320.28 (on a 28-oxygens anhydrous basis)   (1)

55   T °C = 106.2 [^{IV}Al – 0.88 (XFe – 0.34)] + 17.5 (28-oxygens basis)   (2)

56   T °C = 321.98 [^{IV}Al + 0.133 (0.31 – XFe)] – 61.92 (14-oxygens basis)   (3)

57

58   **Chlorite thermodynamic models**

59   Walshe (1986), Vidal et al. (2005) and Inoue et al. (2009) proposed several thermodynamic or

60   semi-thermodynamic models to estimate *P-T* formation conditions from chlorite

61   compositions. These models differ by the choice of the end-member components and activity-

62   composition relationships, and by the *P-T* data used to constrain the activity models.

63   Moreover, Walshe (1986) and Inoue et al. (2009) neglected the non-ideal contributions,

64   whereas Vidal et al. (2005) considered them. In fact the non-ideal nature of the di-

65   trioctahedral substitution is responsible for a miscibility gap between the di/trioctahedral

66   sudoite and the tri/trioctahedral clinochlore-daphnite chlorite end-members. In Vidal et al.

67   (2005), symmetric interactions were assumed as Margules parameters for W_{AlMg}, W_{AlFe}, $W_{\square Fe}$,

68    $W_{\square Mg}$ and $W_{\square Al}$ are determined by calculation and experimentation (e.g. Vidal et al. 2001,

69   2006; Parra et al. 2005). The calculation of the ideal part of end-member activities requires

70   the distribution of cations in the structure to be specified. According to the chlorite structure

71 (Bailey 1988; Holland et al. 1998) with 6 types of sites identified (tetrahedral sites, T1 (x2)

72 and T2 (x2); octahedral sites, M1, M2 (x2), M3 (x2) and M4, with M3-M4 in the brucite

73 sheet), two assumptions are possible: the ordered distribution (Vidal et al. 2005) or the

74 random mixing (Walshe 1986).

75   **Vidal et al. (2005, 2006) model.** Vidal et al. (2001) first proposed a chlorite model

76 based on thermodynamic data. The model was subsequently rearranged by Vidal et al. (2005),

77 with addition of the Fe-amesite end-member, and then by Vidal et al. (2006), with

78 modification of some thermodynamic parameters. These authors suggested that the chlorites

79 are partially ordered. With this ordered model, they assumed that ^{IV}Al is restricted to T2,

80 vacancies to M1, ^{VI}Al fills M4 first then M1 and eventually M2-M3, Fe-Mg fills M2-M3 then

81 M1. In addition, the Fe/Mg ratio is considered equal in the M1 and M2-M3 sites. Vidal et al.

82 (2005) focused on metamorphic chlorites where Si < 3 apfu (O = 14) and on the chlorite +

83 quartz assemblage. They chose 5 appropriate end-member components (Table of appendix 4):

84 clinochlore (Clin), daphnite (Daph), Fe-amesite (Fe-Am), Mg-amesite (Mg-Am) and Mg-

85 sudoite (Mg-Sud). The Fe-sudoite component was not further considered, because of the lack

86 of thermodynamic and experimental data. Thus, Vidal et al. (2005, 2006) constrained a

87 thermobarometer on the basis of the chlorite + quartz assemblage using the following

88 equilibria:

89

90 $2 \text{ Clin} + 3 \text{ Mg-Sud} = 4 \text{ Mg-Am} + 7 \text{ Qz} + 4 \text{ H}_2\text{O}$ (4)

91 $4 \text{ Clin} + 5 \text{ Fe-Am} = 4 \text{ Daph} + 5 \text{ Mg-Am}$ (5)

92 $16 \text{ Daph} + 15 \text{ Mg-Sud} = 20 \text{ Fe-Am} + 6 \text{ Clin} + 35 \text{ Qtz} + 20 \text{ H}_2\text{O}$ (6)

93 $4 \text{ Daph} + 6 \text{ Mg-Sud} = 5 \text{ Fe-Am} + 3 \text{ Mg-Am} + 14 \text{ Qtz} + 8 \text{ H}_2\text{O}$ (7)

94
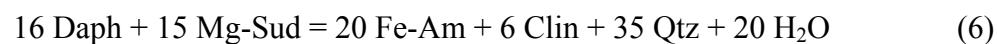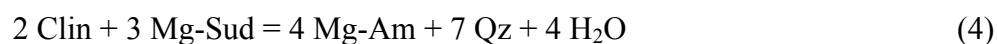
95   Vidal et al. (2005) and Vidal et al. (2006) propose to estimate a minimum $XFe^{3+} = Fe^{3+}/Fe_{total}$

96   based on the achievement of convergence of reactions 4 to 7 at a given pressure, and a

97   maximum XFe^{3+} when the equilibrium convergence is lost. Vidal et al. (2006) have shown

98   that the minimum Fe^{3+} content calculated in this way was compatible with qualitative XANES

99   measurements and can be used as an approximation of the actual Fe^{3+} content. Moreover, the

100 difference between estimates of the minimum and maximum XFe^{3+} ratios is small in the low-

101 T contexts. In order to apply Vidal et al. (2005, 2006) formalism, we assumed that $a_{qz} = 1$ and

102 $a_{H2O} = 1$, which is ensured by the presence of quartz and seems reasonable for low-T chlorite

103 of diagenetic and hydrothermal origin (Inoue et al. 2009), and accounts for the low-carbonate

104 content in the rocks.

105   **Walshe (1986) model.** Walshe (1986) developed an ideal model with an ordered

106 cation distribution in tetrahedral sites and a disordered distribution in octahedral sites, with

107 ^{IV}Al restricted to T2 sites and Fe-Mg-^{VI}Al in M* sites. He proposed a chlorite solid-solution

108 thermometer (Table of appendix 4) with Al-free chlorite (Afch), clinochlore (Clin), chamosite

109 (Chm), and pyrophyllite-gibbsite (Pyr) as end-members, and assuming ideal activities. This

110 choice of end-members ignores Si-poor compositions (Si < 3 apfu) and therefore excludes

111 many low-T chlorite analyses unless, practically, negative mole fractions of the Al-free

112 chlorite component are considered. This established model circumvents the pressure effect,

113 because Walshe (1986) used assumed P data to calculate the thermodynamic parameter of

114 end-members or used analyses of geothermal system samples (Salton Sea and Broadlands). In

115 fact, the chlorite+quartz formation reaction, which is independent of a_{Al}/a^3_{H+} in the fluid, was

116 calibrated, through the equilibrium constant K, on authigenic crystals of the Salton Sea

117 geothermal system, where the pressure variations are negligible compared to temperature

118 variations (Cathelineau 1988). For the chlorite + quartz assemblages, the following

119 equilibrium can be written:

120

121   6 Clin + 14 Qz + 8 $H_2O_{(l)}$ = 5 Afch + 3 Pyr.

122
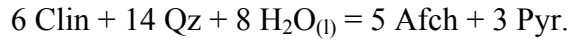
123   If a_{qz} and a_{H2O} are set to 1, the equation becomes a linear relation between T and the chlorite +

124   quartz equilibrium constant as $log\ K$ = A/T + B (with $A = \Delta H/[2.303R]$ and $B = \Delta S/[2.303R]$):

125

126     $$T\degree C = \frac{1626}{6.542 + \frac{1}{3}X} - 273 \text{ where } X = \log K = 5\log a_{ideal}^{Afch} + 3\log a_{ideal}^{Pyr} - 6\log a_{ideal}^{Clin}.$$

127

128   Following the recommandation of Inoue et al. (2009), Fe^{3+} can be assigned to all M* sites in

129   the disordered model of Walshe (1986).

130   **Inoue et al. (2009) model.** Inoue et al. (2009) reappraised the two previous models

131   and suggested that chlorites are disordered at $T < \sim 250$ °C. Following this assumption, the

132   authors calibrated a new thermometer with a random mixing approach. They set the model on

133   temperature, and neglected the pressure effect. Inoue et al. (2009) chose more end-members

134   than Vidal et al. (2005) in order to take into account analyses with Si > 3 apfu. They used the

135   terms 'chamosite' instead of daphnite, 'corundophilite' instead of amesite, as they argued that

136   amesite is a 7 Å phase. They also considered the fictive chlorite component with a serpentine

137   composition defined by Walshe (1986) like Al-free chlorite end-member. The model was

138   calibrated for the magnesian system and finally involved four end-members: Al-free chlorite

139   (Mg-Afch), corundophilite (Crdp), chamosite (Chm) and sudoite (Mg-Sud). As with Walshe

140   (1986), [IV]Al was restricted to T2 sites, and [VI]Al-Fe-Mg were distributed randomly over the

141   M* sites (Table of appendix 4). Inoue et al. (2009) limited the thermometer to the ideal part of

142   activities, leading to the following equation for the formation of the chlorite + quartz

143   assemblage:

144

145   3 Mg-Sud + Mg-Afch = 3 Crdp + 7 Qz + 4 H_2O

146
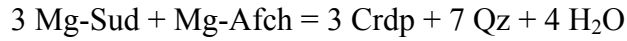
147   and finally to the following expression for *T*, with activities of quartz and water assumed to be

148   1:

149

150    $$T°C = \frac{1}{0.00293 - 0.000513X + 0.00003904X^2} - 273$$

151   where $X = \log K = 3\log a_{ideal}^{Crdp} - 3\log a_{ideal}^{Sud} - \log a_{ideal}^{Afch}$

152

153   The disordered model of Inoue et al. (2009) assumed that Fe^{3+} could be assigned to all M*

154   sites.

155

156   **Illite thermobarometry**

157

158   **Empirical illite thermometer**

159   The chemical composition of illite is mainly dependent on *P, T*, the bulk rock composition

160   and fluid composition. The increasing interlayer content (K + Na + Ca) is often correlated to

161   the increase of burial *P-T* conditions. This reflects the phenomenon of illitization, which

162   transforms a low-charge smectite into a high-charge illite (e.g. Cathelineau and Nieva 1985;

163   Lanson and Besson 1992; Battaglia 2004; Dubacq et al. 2010). The presence of interlayer

164   vacancies is accounted for by the introduction of a pyrophyllite end-member in the mica solid

165   solution. Cathelineau (1988) observed, on samples from three different geothermal fields, a

166   trend between interlayer occupancy and temperature, described by the following equation:

167

168 $$T°C = \frac{-XPyr + 0.7928}{0.0025}$$

169

170 where XPyr represents the pyrophyllite molar fraction, calculated from the substitution vector

171 $K_{-1}^{IV}[SiAl]$. Actually, the molar fraction calculation of each end-member is more complex

172 and must take into account all observed substitution vectors simultaneously. From a chemical

173 point of view, Cathelineau (1988) underlined the difficulty to find a general trend between the

174 temperature of crystallization and the cation occupancy. He showed that each studied

175 geothermal field (Los Azufres, Coso and Salton Sea) has its own evolution of K content with

176 temperature and concluded that no general relation between the mineral composition and the

177 temperature of crystallization could be proposed. However, Battaglia (2004) proposed an

178 empirical illite thermometer directly based on K content with a new correction accounting for

179 the Fe-Mg content:

180

181 T °C = 267.95 (K + |Fe - Mg|) + 31.50 (11 oxygens basis).

182

183 The author claimed that this relation is applicable for all geothermal fields, with an error on

184 temperature calculation around 7%. In this case, the Fe-Mg content is considered as an

185 indicator of the variation of rock composition.

186

187 **Illite thermodynamic model of Dubacq et al. (2010)**

188 Parra et al. (2002) proposed and calibrated a model representing the phengite-quartz

189 equilibrium, calculated from activity of chosen end-members and taking into account the non-

190 ideal part of activity coefficients. Dubacq et al. (2010) extended this model to smectite, illite,

191 interlayered smectite-illite and mica by considering the *T*–hydration relationship, the pressure

192 and the rock composition, and using multi-equilibrium thermobarometry. This model was the

193   first attempt to provide a unique set of 2:1 phyllosilicates thermodynamic properties in a

194   solid-solution model relevant from diagenetic to metamorphic conditions.

195   Six substitutions are identified in the smectite-illite-mica compositional field, the Tschermak,

196   the ferro-magnesian, the di-trioctahedral, the $^{VI}Al = Fe^{3+}$, the paragonitic ($^{XII}K = {}^{XII}Na$), and

197   the pyrophyllitic ($^{XII}[Na,K] {}^{IV}Al = {}^{XII}\square{}^{IV}Si$) substitutions, where IV, VI and XII indicate

198   tetrahedral, octahedral and interlayer sites, respectively. The model involves nine end-

199   members, one of which has several levels of hydration (Table of appendix 4): muscovite

200   (Musc), paragonite (Pg), Mg-celadonite (Mg-Cel), Fe-celadonite (Fe-Cel), phlogopite (Phl),

201   annite (Ann), pyrophyllite (Prl), hydrated pyrophyllite (Prl·$1H_2O$, ·$2H_2O$, ·$4H_2O$, ·$7H_2O$) and

202   margarite (Mrg).

203   To calculate the activity of each end-member, six types of crystallographic sites were

204   considered according to the 2:1 phyllosilicates ideal structure: T1 (x2) and T2 (x2) tetrahedral

205   sites, M2 (x2), M3 (x2) and M1 octahedral sites, and A* interlayer sites, with A1, A2, A3 and

206   A4 corresponding to the different interlayer sheets according to the hydration and water

207   layers. Moreover, an ordered distribution of cation was assumed: ^{IV}Al is restricted to T2, ^{VI}Al

208   to M2-M3 and vacancies to M1. Fe and Mg have a preference for the M1 sites, but they can

209   also occupy the M2-M3 sites. Finally, K, Na, Ca and water are only assigned to A* sites.

210   According to the results obtained previously by Parra et al. (2002), Dubacq et al. (2010)

211   considered the non-ideality of cationic exchanges by using symmetric Margules parameters

212   on M1 and A sites only for $W_{\square K}$ and $W_{\square Na}$, and with asymmetric Margules parameters on A in

213   the others cases. Three independent equilibria and their hydrated equivalent can be written for

214   any smectite, illite or mica + quartz + water equilibrium:

215

216    $3\ MgCel·mH_2O + 2\ Prl·(m+1)H_2O = 2\ Musc·mH_2O + Phl·mH_2O + 11Qz + (2m+4)H_2O$

217    $3\ FeCel·mH_2O + 2\ Prl·(m+1)H_2O = 2\ Musc·mH_2O + Ann·mH_2O + 11Qz + (2m+4)H_2O$

218 Prl·$(m+1)$H$_2$O$_{nw}$ = Prl·$(m'+1)$H$_2$O$_{nw}$ + $(m - m')$H$_2$O

219

220 where $(m+1)$ and $(m'+1)$ are the maximum and minimum amount of water in interlayer, with

221 m and m' varying from 0 to 6 and 0 to 3 according to the number of water layers (noted nw).

222 A pressure–temperature relation is obtained simultaneously with the hydration state.

223 A scanning transmission X-ray microscopy (STXM) and X-ray absorption near edge-structure

224 (XANES) study of Bourdelle (2011, *PhD*) showed that phyllosilicates of the Gulf Coast have

225 a $Fe^{3+}/(Fe^{3+} + Fe^{2+})$ ratio higher than 50%. Taking ferric iron into account implies an increase

226 of calculated vacancies. Fe^{3+} is assumed to replace ^{VI}Al, and is therefore restricted to the M2-

227 M3 sites in Dubacq et al. (2010) model.

228

229   **Illite-chlorite assemblages**

230

231 **Walshe (1986) model**

232 Walshe (1986) envisaged a heterogeneous equilibrium between one chlorite and one mica

233 end-member defining a chlorite + mica + quartz + K-feldspar + water equilibrium. The author

234 chose to represent the mica phase with a muscovite structure and a random-mixing cation

235 distribution and ideal activities (Table of appendix 4). Walshe (1986) calibrated the following

236 reaction:

237

238 6 Clin + 6 K-Feld + 2 Qz + 2 H$_2$O = 6 Musc + 5 Mg-Afch.

239
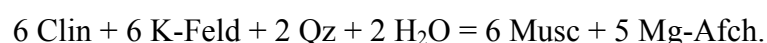
240 Assuming that $a_{Qz} = a_{K\text{-feld}} = a_{H2O} = 1$, a new thermometer is defined as:

241

242     $T°C = \dfrac{-1113}{-0.575 + \dfrac{1}{6}X} - 273$ with $X = \log K = 5\log a_{ideal}^{Mg-Afch} + 6\log a_{ideal}^{Musc} - 6\log a_{ideal}^{Clin}$.

243

244   **Multi-equilibrium approach: combination of Vidal et al. (2005, 2006) and Dubacq et al.**

245   **(2010) models**

246   The non-ideal ordered models for illite-micas (Dubacq et al. 2010) and chlorites (Vidal et al.

247   2005, 2006) can be used simultaneously to deduce T and P simultaneously, assuming the

248   achievement of local equilibrium between chlorites and illites. This is what was applied in

249   this study to a series of Gulf coast samples.

250

251   **References**

252

253   Bailey, S.W. (1988) Chlorites: structures and crystal chemistry. In S.W. Bailey, Eds.,

254   Hydrous Phyllosilicates (Exclusive of Micas), p. 347-403. Mineralogical Society of America,

255   Washington D.C.

256   Battaglia, S. (2004) Variations in the chemical composition of illite from five geothermal

257   fields: a possible geothermometer. Clay Minerals, 39, 501-510.

258   Bourdelle, F. (2011) Thermobarométrie des phyllosilicates dans les séries naturelles:

259   Conditions de la diagenèse et du métamorphisme de bas degré, 318 p. Ph.D. thesis, University

260   Paris-Sud, Orsay.

261   Cathelineau, M. (1988) Cation site occupency in chlorites and illites as a function of

262   temperature. Clay Minerals, 23, 471-485.

263   Cathelineau, M. and Nieva, D. (1985) A chlorite solid solution geothermometer. The Los

264   Azufres (Mexico) geothermal system. Contributions to Mineralogy and Petrology, 91, 235-

265   244.

266   De Caritat, P., Hutcheon, I., and Walshe, J.L. (1993) Chlorite geothermometry: a review.

267   Clays and Clay Minerals, 41, 219-239.

268   Dubacq, B., Vidal, O., and De Andrade, V. (2010) Dehydration of dioctahedral aluminous

269   phyllosilicates: thermodynamic modelling and implications for thermobarometric estimates.

270   Contributions to Mineralogy and Petrology, 159, 159-174.

271   Essene, E.J. and Peacor, D.R. (1995) Clay mineral thermometry - A critical perspective. Clays

272   and Clay Minerals, 43, 540-553.

273   Hillier, S. and Velde, B. (1991) Octahedral Occupancy and the Chemical-Composition of

274   Diagenetic (Low-Temperature) Chlorites. Clay Minerals, 26, 149-168.

275   Holland, T.J.B., Baker, J., and Powell, R. (1998) Mixing properties and activity composition

276   relationships of chlorites in the system $MgO-FeO-Al_2O_3-SiO_2-H_2O$. European Journal of

277   Mineralogy, 10, 395-406.

278   Inoue, A., Meunier, A., Patrier-Mas, P., Rigault, C., Beaufort, D., and Vieillard, P. (2009)

279   Application of Chemical Geothermometry to Low-Temperature Trioctahedral Chlorites.

280   Clays and Clay Minerals, 57, 371-382.

281   Jiang, W.T., Peacor, D.R., and Buseck, P.R. (1994) Chlorite Geothermometry -

282   Contamination and Apparent Octahedral Vacancies. Clays and Clay Minerals, 42, 593-605.

283   Jowett, E.C. (1991) Fitting iron and magnesium into the hydrothermal chlorite

284   geothermometer. GAC/MAC/SEG Joint annual meeting, Toronto, Canada.

285   Kranidiotis, P. and McLean, W.H. (1987) Systematics of chlorite alternation at the Phelps

286   Dodge massive sulfide deposit, Matagami, Quebec. Economic Geology, 82, 1898-1911.

287   Lanson, B. and Besson, G. (1992) Characterization of the End of Smectite-to-Illite

288   Transformation - Decomposition of X-Ray-Patterns. Clays and Clay Minerals, 40, 40-52.

289   Parra, T., Vidal, O., and Agard, P. (2002) A thermodynamic model for Fe-Mg dioctahedral K

290   white micas using data from phase-equilibrium experiments and natural pelitic assemblages.

291   Contributions to Mineralogy and Petrology, 143, 706-732.

292   Parra, T., Vidal, O., and Theye, T. (2005) Experimental data on the Tschermak substitution in

293   Fe-chlorite. American Mineralogist, 90, 359-370.

294   Shau, Y.H., Peacor, D.R., and Essene, E.J. (1990) Corrensite and mixed-layer

295   chlorite/corrensite in metabasalt from northern Tawaïn: TEM/AEM, EMPA, XRD and optical

296   studies. Contributions to Mineralogy and Petrology, 105, 123-142.

297   Vidal, O., De Andrade, V., Lewin, E., Munoz, M., Parra, T., and Pascarelli, S. (2006) P-T-

298   deformation-Fe^{3+}/Fe^{2+} mapping at the thin section scale and comparison with XANES

299   mapping: application to a garnet-bearing metapelite from the Sambagawa metamorphic belt

300   (Japan). Journal of Metamorphic Geology, 24, 669-683.

301   Vidal, O., Parra, T., and Trotet, F. (2001) A thermodynamic model for Fe-Mg aluminous

302   chlorite using data from phase equilibrium experiments and natural pelitic assemblages in the

303   100 degrees to 600 degrees C, 1 to 25 kb range. American Journal of Science, 301, 557-592.

304   Vidal, O., Parra, T., and Vieillard, P. (2005) Thermodynamic properties of the Tschermak

305   solid solution in Fe-chlorite: Application to natural examples and possible role of oxidation.

306   American Mineralogist, 90, 347-358.

307   Walshe, J.L. (1986) A six-component chlorite solid solution model and the conditions of

308   chlorite formation in hydrothermal and geothermal systems. Economic Geology, 81, 681-703.

309   Xie, X.G., Byerly, G.R., and Ferrell, R.E. (1997) IIb trioctahedral chlorite from the Barberton

310   greenstone belt: Crystal structure and rock composition constraints with implications to

311   geothermometry. Contributions to Mineralogy and Petrology, 126, 275-291.

312   Zang, W. and Fyfe, W.S. (1995) Chloritization of the Hydrothermally Altered Bedrock at the

313   Igarape-Bahia Gold Deposit, Carajas, Brazil. Mineralium Deposita, 30, 30-38.

314 **Table of appendix 4:** Ideal activities of solid-solution components used in the calculation of

315 the thermobarometers for chlorite and illite. $X_{j,s}$ is the mole fraction of the j cation on the s

316 site.

317

End-members (abbreviations)	Chemical formulae	Ideal activities
Vidal et al. *(2005) model – Chl+Qz*		
Clinochlore (Clin)	$(AlMg_5)(Si_3Al)O_{10}(OH)_8$	$a_{Clin} = 4\ (X_{Mg,M1})(X_{Mg,M2+M3})^4(X_{Si,T2})(X_{Al,T2})$
Daphnite (Daph)	$(AlFe_5)(Si_3Al)O_{10}(OH)_8$	$a_{Daph} = 4\ (X_{Fe,M1})(X_{Fe,M2+M3})^4(X_{Si,T2})(X_{Al,T2})$
Mg-Amesite (Mg-Am)	$(Al_2Mg_4)(Si_2Al_2)O_{10}(OH)_8$	$a_{Mg-Sud} = 64\ (X_{\square,M1})(X_{Al,M2+M3})^2(X_{Mg,M2+M3})^2(X_{Si,T2})(X_{Al,T2})$
Fe-Amesite (Fe-Am)	$(Al_2Fe_4)(Si_2Al_2)O_{10}(OH)_8$	$a_{Fe-Sud} = 64\ (X_{\square,M1})(X_{Al,M2+M3})^2(X_{Fe,M2+M3})^2(X_{Si,T2})(X_{Al,T2})$
Mg-Sudoite (Mg-Sud)	$(Al_3Mg_2)(Si_3Al)O_{10}(OH)_8$	$a_{Mg-Am} = (X_{Al,M1})(X_{Mg,M2+M3})^4(X_{Al,T2})^2$
Walshe (1986) model – Chl+Qz		
Al-free Chlorite (Mg-Afch)	$(Mg_6)(Si_4)O_{10}(OH)_8$	$a_{Mg-Afch} = (X_{Mg,oct})^6(X_{Si,tet})^2$
Clinochlore (Clin)	$(AlMg_5)(Si_3Al)O_{10}(OH)_8$	$a_{Clin} = 59.720\ (X_{Mg,oct})^5(X_{Al,oct})(X_{Al,tet})\ (X_{Si,tet})$
Chamosite (Chm = Daph)	$(AlFe_5)(Si_3Al)O_{10}(OH)_8$	$a_{Chm} = 59.720\ (X_{Fe,oct})^5(X_{Al,oct})(X_{Si,tet})(X_{Al,tet})$
Pyrophyllite-Gibbsite (Pyr)	$(Al_4)(Si_4)O_{10}(OH)_8$	$a_{Pyrophyllite} = X_{pyrophyllite} = 5 - \Sigma(cations_{tet+oct})/2$
Muscovite (Musc) – *Chl+Musc+Qz*	$K(Al_2)(Si_3Al)O_{10}(OH)_2$	$a_{Musc} = 27\ (X_{Al,\ oct})^2(X_{\square,\ oct})(X_{Si,\ tet})(X_{Al,\ tet})(X_{K,\ A})$
Inoue et al. *(2009) model – Chl+Qz*		
Al-free Chlorite (Mg-Afch)	$(Mg_6)(Si_4)O_{10}(OH)_8$	$a_{Mg-Afch} = (X_{Mg,oct})^6(X_{Si,tet})^2$
Chamosite (Chm = Daph)	$(AlFe_5)(Si_3Al)O_{10}(OH)_8$	$a_{Chm} = 59.720\ (X_{Fe,oct})^5(X_{Al,oct})(X_{Si,tet})(X_{Al,tet})$
Corundophilite (Crdp = Mg-Am)	$(Al_2Mg_4)(Si_2Al_2)O_{10}(OH)_8$	$a_{Crdp} = 45.563\ (X_{Mg,oct})^4(X_{Al,oct})^2(X_{Al,tet})^2$
Mg-Sudoite (Mg-Sud)	$(Al_3Mg_2)(Si_3Al)O_{10}(OH)_8$	$a_{Mg-Sud} = 1728\ (X_{Mg,oct})^2(X_{Al,oct})^3(X_{\square,oct})(X_{Si,tet})(X_{Al,tet})$
Dubacq et al. *(2010) model – Chl+Qz*		
Muscovite (Musc)	$K(Al_2)(Si_3Al)O_{10}(OH)_2$	$a_{Musc} = 4\ (X_{Al,\ M2+M3})^2(X_{\square,\ M1})(X_{Si,\ T2})(X_{Al,\ T2})(X_{K,\ A})$
Paragonite (Pg)	$Na(Al_2)(Si_3Al)O_{10}(OH)_2$	$a_{Pg} = 4\ (X_{Al,\ M2+M3})^2(X_{\square,\ M1})(X_{Si,\ T2})(X_{Al,\ T2})(X_{Na,\ A})$
Mg-Celadonite (Mg-Cel)	$K(AlMg)(Si_4)O_{10}(OH)_2$	$a_{MgCel} = 4\ (X_{Mg,\ M2+M3})(X_{\square,\ M1})(X_{Si,\ T2})^2(X_{Al,\ T2})(X_{K,\ A})$
Fe-Celadonite (Fe-Cel)	$K(AlFe)(Si_4)O_{10}(OH)_2$	$a_{FeCel} = 4\ (X_{Fe,\ M2+M3})(X_{\square,\ M1})(X_{Si,\ T2})^2(X_{Al,\ T2})(X_{K,\ A})$
Phlogopite (Phl)	$K(Mg_3)(Si_2Al)O_{10}(OH)_2$	$a_{Ann} = 4\ (X_{Fe,\ M2+M3})^2(X_{Fe,\ M1})(X_{Si,\ T2})(X_{Al,\ T2})(X_{K,\ A})$
Annite (Ann)	$K(Fe_3)(Si_2Al)O_{10}(OH)_2$	$a_{Phl} = 4\ (X_{Mg,\ M2+M3})^2(X_{Mg,\ M1})(X_{Si,\ T2})(X_{Al,\ T2})(X_{K,\ A})$
Pyrophyllite (Prl)	$(Al_2)(Si_4)O_{10}(OH)_2$	$a_{Prl} = (X_{Al,\ M2+M3})^2(X_{\square,\ M1})(X_{Si,\ T2})^2(X_{\square,\ A})$
Hydrated Pyrophyllite (Prl·mH$_2$O)	$(Al_2)(Si_4)O_{10}(OH)_2 . nH_2O$	$a_{Prl,mH2Onw} = (X_{Al,\ M2+M3})^2(X_{v,\ M1})(X_{Si,\ T2})^2 \prod(X_{H2O,\ An})(X_{\square,\ An+1})$

318

319